

# Donut and dynamic polarization effects in proton channeling through carbon nanotubes

D Borcka<sup>1‡</sup>, D J Mowbray<sup>2</sup>, Z L Mišković<sup>3</sup>, S Petrović<sup>1</sup> and N Nešković<sup>1</sup>

<sup>1</sup> Laboratory of Physics (010), Vinča Institute of Nuclear Sciences, P.O. Box 522, 11001 Belgrade, Serbia

<sup>2</sup> Department of Physics, Center for Atomic-scale Materials Design (CAMD), Technical University of Denmark, DK-2800 Kgs. Lyngby, Denmark

<sup>3</sup> Department of Applied Mathematics, University of Waterloo, Waterloo, Ontario, Canada N2L3G1

E-mail: [dusborcka@vinca.rs](mailto:dusborcka@vinca.rs)

**Abstract.** We investigate the angular and spatial distributions of protons of the energy of 0.223 MeV after channeling through an (11, 9) single-wall carbon nanotube of the length of 0.2  $\mu\text{m}$ . The proton incident angle is varied between 0 and 10 mrad, being close to the critical angle for channeling. We show that, as the proton incident angle increases and approaches the critical angle for channeling, a ring-like structure is developed in the angular distribution - donut effect. We demonstrate that it is the rainbow effect. When the proton incident angle is between zero and a half of the critical angle for channeling, the image force affects considerably the number and positions of the maxima of the angular and spatial distributions. However, when the proton incident angle is close to the critical angle for channeling, its influence on the angular and spatial distributions is reduced strongly. We demonstrate that the increase of the proton incident angle can lead to a significant rearrangement of the propagating protons within the nanotube. This effect may be used to locate atomic impurities in nanotubes as well as for creating nanosized proton beams to be used in materials science, biology and medicine.

Submitted to: *New J. Phys.*

**Contents**

<b>1</b>	<b>Introduction</b>	<b>2</b>
<b>2</b>	<b>Theory</b>	<b>4</b>
<b>3</b>	<b>Results and discussion</b>	<b>6</b>
<b>4</b>	<b>Concluding remarks</b>	<b>14</b>

**1. Introduction**

While the progress in theoretical modeling and computer simulation of ion channeling through carbon nanotubes has reached a mature level, as reviewed in Refs. [1]–[10], the experimental advancement in this area is still in its infancy. Since the issues of ordering, straightening and holding nanotubes are probably the most challenging tasks in the experimental realization of ion channeling through them, it is not a surprise that the best results in performing these tasks are expected when they are grown in a dielectric medium. For example, the first experimental data on ion channeling through nanotubes, which were reported by Zhu et al. [11], were obtained with the  $He^+$  ions and array of well-ordered multi-wall nanotubes grown in a porous anodic aluminum oxide ( $Al_2O_3$ ) membrane. The authors performed and compared the results of direct measurements of the yield of ions transmitted through the bare  $Al_2O_3$  sample and the  $Al_2O_3$  sample with nanotubes.

On the other hand, the first experimental results on electron channeling through carbon nanotubes were reported by Chai et al. [12]. The authors studied the transport of electrons of the energy of 300 keV through the aligned multi-wall nanotubes of the lengths of 0.7-3.0  $\mu m$  embedded in the carbon fiber coatings. The misalignment of the nanotubes was up to  $1^\circ$ . Besides, Berdinsky et al. [13] succeeded in growing the single-wall carbon nanotubes (SWCNTs) in the ion tracks etched in the  $SiO_2$  layers on a Si substrate, offering an interesting possibility for the experimental realization of ion channeling through nanotubes in a wide range of ion energies.

Regarding the theoretical modeling and computer simulation of ion channeling through carbon nanotubes, we note that the effect of dynamic polarization of the nanotube atoms valence electrons by the ion is not usually taken into account [1]–[14] since its influence at very low and very high energies, of the orders of 1 keV and 1 GeV, respectively, is negligible. However, it is expected that at medium energies, of the order of 1 MeV, this effect contributes significantly to the ion energy loss and gives rise to an additional force acting on the ions, called the image force [15, 16], as it has been demonstrated in the computer simulation of the angular distributions of protons channeled through the SWCNTs in vacuum [17]. The importance of the image force has also been emphasized in the related area of ion transmission through cylindrical channels in metals [18]–[23] and on ions and molecules moving over supported graphene

[24, 25].

When the ion channeling dynamics at very low and very high energies is concerned, the material surrounding the carbon nanotubes serves predominantly as their passive container. However, the ions moving at medium energies induce the strong dynamic polarization of both the nanotube atoms valence electrons and the surrounding material, which in turn gives rise to a sizeable image force [26, 27]. In these two studies, the image force was calculated by a two-dimensional (2D) hydrodynamic model of the nanotube atoms valence electrons while the surrounding material was described by a frequency dependent dielectric function. On the other hand, the image force has recently been shown to influence significantly the rainbow effect in proton channeling through the short SWCNTs [28] and double-wall nanotubes in vacuum [29] as well as through the short SWCNTs in the dielectric media [30, 31]. We think that it is important to improve our understanding of the role of the image force in the rainbow effect with nanotubes because, in analogy with the case of surface ion channeling [32]–[34], the measurements of this effect can give precise information on both the atomic configuration and interaction potentials within nanotubes, which have not yet been explored completely.

However, in ion channeling experiments, the always present questions are the ones of ion beam divergence and misalignment. So, it is important to study the influence of the effect of dynamic polarization of carbon nanotubes when the initial ion velocity is not parallel to the nanotube axis. Therefore, in this paper, we continue our investigation of the image force with the case in which the ion incident angle is not zero. Specifically, we analyze the angular and spatial distributions of protons of the velocity of 3 a.u. channeled through the straight (11, 9) SWCNTs of the length of 0.2  $\mu\text{m}$  in vacuum. The proton incident angle is varied between 0 and 10 mrad, being close to the critical angle for channeling. This proton velocity is chosen because the dynamic polarization effect is the strongest in the range about it. The consideration is limited to the case of a nanotube in vacuum because the presence of a dielectric medium around it would introduce only a slight modifying factor in the results of calculation [30, 31].

It is well known that, for the ion incident angles close to the critical angle for channeling, the donut effect develops in the angular distributions of channeled ions. The effect was measured with the Si and Ge crystals [35]–[37], and explained independently afterwards by the theory of crystal rainbows [38, 39]. That theory was formulated as a proper theory of ion channeling through thin crystals [40], and has been applied subsequently to ion channeling through short carbon nanotubes [41]–[44]. It must be noted that the donut effect has also been observed in a computer simulation of ion propagation through nanotubes [45]. However, the authors did not connect the obtained results to the rainbow effect. We explore here the donut effect in the angular and spatial distributions of protons channeled through a (11, 9) SWCNT in the presence of the image force.

Regarding the angular and spatial distributions of channeled protons to be presented in this study, corresponding to the case in which the proton incident angle is not zero, we note that the proton equations of motion in the transverse position plane

that are solved to generate them are 2D. This means that the case we explore is truly 2D, unlike the cases treated in our previous studies of the image force in carbon nanotubes, which were in fact one-dimensional (1D) [28]–[31].

The atomic units will be used throughout the paper unless explicitly stated otherwise.

## 2. Theory

We adopt the right Cartesian coordinate system with the  $z$  axis coinciding with the nanotube axis, the origin in the entrance plane of the nanotube, and the  $x$  and  $y$  axes the vertical and horizontal axes, respectively. The initial proton velocity,  $\vec{v}$ , is taken to lie in the  $yz$  plane and make angle  $\varphi$  with the  $z$  axis, being the proton incident angle. The length of the nanotube,  $L$ , is assumed to be large enough to allow us to ignore the influence of the nanotube edges on the image force, and, at the same time, small enough to neglect the energy losses of channeled protons.

We assume that the interaction between the proton and nanotube atoms can be treated classically using the Doyle-Turner expression [46] averaged axially [47] and azimuthally [45]. This interaction is repulsive and of the short-range character. Thus, the repulsive interaction potential in the proton channeling through the nanotube is of the form

$$U_{\text{rep}}(r) = \frac{32\pi dZ_1Z_2a}{3\sqrt{3}l^2} \times \sum_{j=1}^4 a_j b_j^2 I_0(2ab_j^2 r) \exp\{-b_j^2[r^2 + a^2]\}, \quad (1)$$

where  $Z_1 = 1$  and  $Z_2 = 6$  are the atomic numbers of the hydrogen and carbon atoms, respectively,  $a$  is the nanotube radius,  $l$  is the nanotube atoms bond length,  $r = (x^2 + y^2)^{\frac{1}{2}}$  is the distance between the proton and nanotube axis,  $I_0$  is the modified Bessel function of the 1<sup>st</sup> kind and 0<sup>th</sup> order, and  $a_j = \{0.115, 0.188, 0.072, 0.020\}$  and  $b_j = \{0.547, 0.989, 1.982, 5.656\}$  are the fitting parameters (in atomic units) [46].

The dynamic polarization of the nanotube by the proton is treated via a 2D hydrodynamic model of the nanotube atoms valence electrons, based on a jellium-like description of the ion cores making the nanotube wall [15]–[26]. This model includes the axial and azimuthal averaging similar to that applied in obtaining the corresponding repulsive interaction potential, given by Eq. (1). It finally gives the interaction potential between the proton and its image,  $U_{\text{im}}(r, t)$ , which is stationary in the coordinate system moving with the proton and depends on its velocity. This interaction is attractive and of the long-range character. The details of derivation of the expression for  $U_{\text{im}}(r, t)$  are given elsewhere [15]–[30]. Consequently, the total interaction potential in the proton channeling through the nanotube is

$$U(r, t) = U_{\text{rep}}(r) + U_{\text{im}}(r, t). \quad (2)$$

The proton equations of motion we solve are

$$m\ddot{x}(t) = -\frac{\partial U(r, t)}{\partial x}, \quad (3)$$

$$m\ddot{y}(t) = -\frac{\partial U(r, t)}{\partial y}, \quad (4)$$

where  $m$  is the proton mass. They are subject to the initial conditions for the transverse components of the proton velocity that are

$$\dot{x}(t = 0) = 0, \quad (5)$$

$$\dot{y}(t = 0) = v \sin \varphi \approx v\varphi. \quad (6)$$

The longitudinal proton motion is treated as uniform with the initial condition for the longitudinal component of the proton velocity that is  $\dot{z}(t = 0) = v \cos \varphi \approx v$ . As a result, the longitudinal component of the proton position is  $z(t) = vt$ . Equations (5) and (6) are solved numerically. The angular and spatial distributions of transmitted protons are generated using a Monte Carlo computer simulation code. The components of the proton impact parameter,  $x_0$  and  $y_0$ , are chosen randomly from a uniform distribution within the cross-sectional area of the nanotube and its entrance plane. With  $l = 0.144$  nm [48], we obtain that  $a = 0.689$  nm. If the proton impact parameter falls inside annular interval  $[a - a_{sc}, a]$ , where  $a_{sc} = [9\pi^2/(128Z_2)]^{1/3}a_0$  is the screening radius and  $a_0$  the Bohr radius, the proton is treated as if it is backscattered and is disregarded. The initial number of protons is about 1 000 000.

The components of the proton scattering angle,  $\Theta_x$  and  $\Theta_y$ , are obtained via expressions  $\Theta_x = V_x/v$  and  $\Theta_y = V_y/v$ , where  $V_x$  and  $V_y$  are the final transverse components of the proton velocity, which are obtained, together with the final transverse components of the proton position,  $X$  and  $Y$ , as the solutions of Eqs. (5) and (6). The proton channeling through the nanotube can be analyzed via the mapping of the impact parameter plane, the  $x_0y_0$  plane, to the scattering angle plane, the  $\Theta_x\Theta_y$  plane [40]. The corresponding total interaction potential, given by Eq. (2), is axially symmetric. This means that, if the initial proton velocities were parallel to the nanotube axis, this mapping would be 1D. However, the initial proton velocities are not parallel to the nanotube axis, and the mapping is 2D. Since the proton scattering angle is small, its differential transmission cross section is given by

$$\sigma = -\frac{1}{|J_\Theta|}, \quad (7)$$

where  $J_\Theta$  is the Jacobian of the mapping,

$$J_\Theta = \frac{\partial \Theta_x}{\partial x_0} \frac{\partial \Theta_y}{\partial y_0} - \frac{\partial \Theta_x}{\partial y_0} \frac{\partial \Theta_y}{\partial x_0}. \quad (8)$$

Thus, equation  $J_\Theta = 0$  determines the lines in the impact parameter plane along which the proton differential transmission cross section is singular. The images of these lines in the scattering angle plane are the rainbow lines in this plane [40].

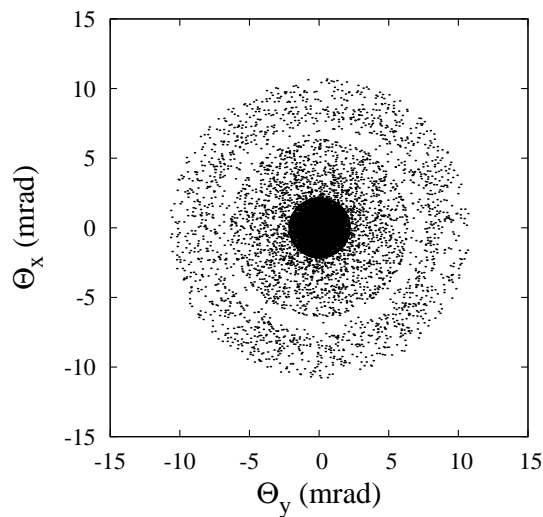


**Figure 1.** The angular distribution of protons channeled in the (11, 9) SWCNT with the inclusion of the image force when the proton incident angle  $\varphi = 0$ . The proton velocity is  $v = 3$  a.u., the nanotube radius  $a = 0.689$  nm, and the nanotube length  $L = 0.2 \mu\text{m}$ .

We can analyze in a similar way the mapping of the impact parameter plane (the  $x_0y_0$  plane), which is the entrance plane of the nanotube and the initial transverse position plane, to the exit plane of the nanotube or the final transverse position plane, the plane. The Jacobian of this mapping is

$$J_R = \frac{\partial X}{\partial x_0} \frac{\partial Y}{\partial y_0} - \frac{\partial X}{\partial y_0} \frac{\partial Y}{\partial x_0}. \quad (9)$$

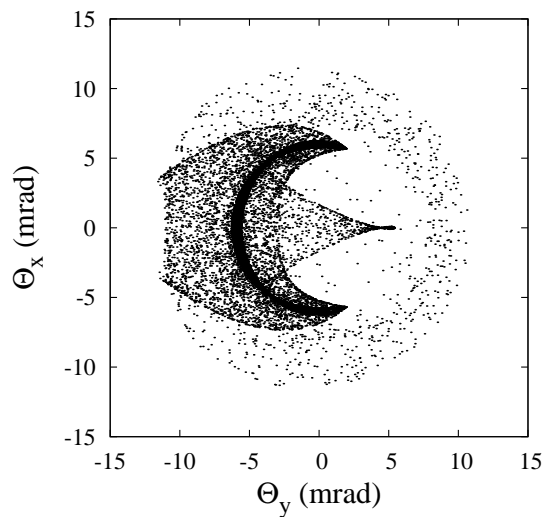
The rainbow lines in the final transverse position plane are the images of the lines in the impact parameter plane determined by equation  $J_R = 0$ .

### 3. Results and discussion

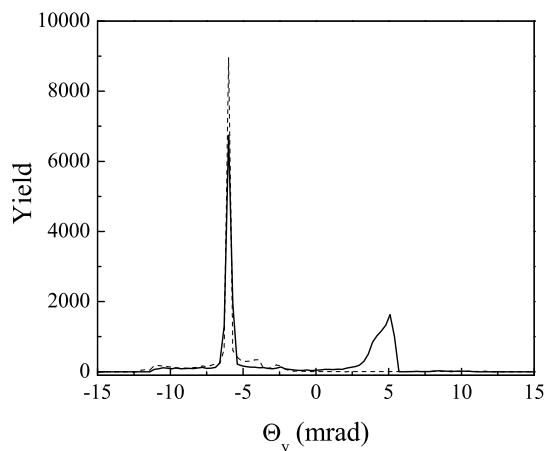
Let us now analyze the angular and spatial distributions of protons channeled in the (11, 9) SWCNT of the length of  $0.2 \mu\text{m}$ . In all the cases to be studied, the initial proton velocity will be  $v = 3$  a.u., corresponding to the initial proton energy of 0.223 MeV, while the incident proton angle,  $\varphi$ , will be varied between 0 and 10 mrad. The maximal proton incident angle will be close to the critical angle for channeling,  $\psi_c$ , being about 11 mrad. The analysis will also include the typical proton trajectories through the nanotube in the proton phase space.

In Figs. 1-6 we shall display the evolution of the angular distribution of channeled protons with the increase of  $\varphi$ . In particular, we shall analyze the development of a ring-like structure in the angular distribution under the influence of the image force.

The scatter plot shown in Fig. 1 represents the angular distribution of channeled protons for  $\varphi = 0$  with the image force included. The corresponding angular distribution without the inclusion of the image force contains in its central part only a maximum

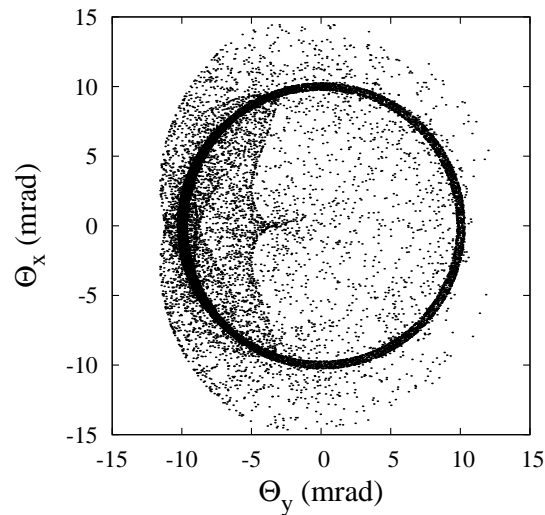


**Figure 2.** The angular distribution of protons channeled in the (11, 9) SWCNT with the inclusion of the image force when the proton incident angle  $\varphi = 6$  mrad. The proton velocity is  $v = 3$  a.u., the nanotube radius  $a = 0.689$  nm, and the nanotube length  $L = 0.2$   $\mu\text{m}$ .

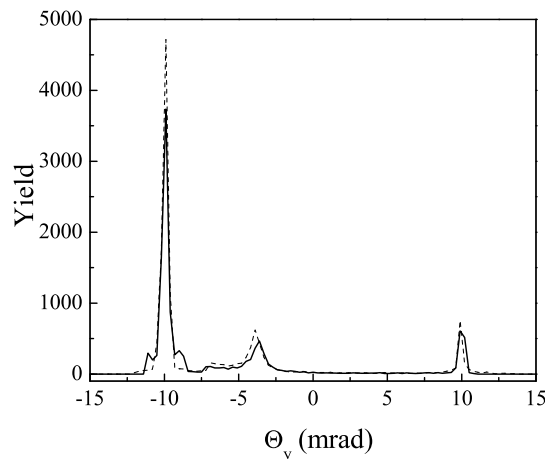


**Figure 3.** The distribution along the  $\Theta_y$  axis of protons channeled in the (11, 9) SWCNT with the image force taken into account – the solid curve – and without it – the dashed curve – when the proton incident angle  $\varphi = 6$  mrad. The proton velocity is  $v = 3$  a.u., the nanotube radius  $a = 0.689$  nm, and the nanotube length  $L = 0.2$   $\mu\text{m}$ . The former curve corresponds to the angular distribution shown in Fig. 2.

at the origin. This means that the non-monotonic character of the central part of the angular distribution with the image force included is due to the effect of dynamic polarization. This was discussed in one of our previous papers [28]. We presented in it the distributions of channeled protons along the  $\Theta_y$  axis (in the scattering angle plane) with and without the image force included, which were in fact (for  $\varphi = 0$ ) the radial yields of channeled protons. The conclusion of the discussion was that the maxima of the radial yield, appearing when the image force was included, were due to the rainbow effect.



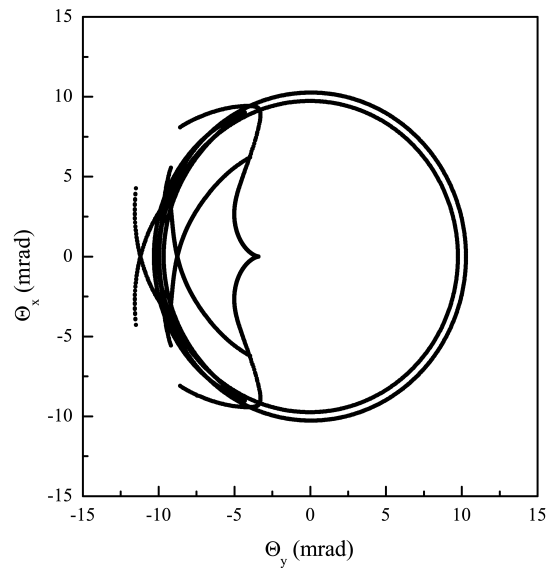
**Figure 4.** The angular distribution of protons channeled in the (11, 9) SWCNT with the inclusion of the image force when the proton incident angle  $\varphi = 10$  mrad. The proton velocity is  $v = 3$  a.u., the nanotube radius  $a = 0.689$  nm, and the nanotube length  $L = 0.2$   $\mu\text{m}$ .



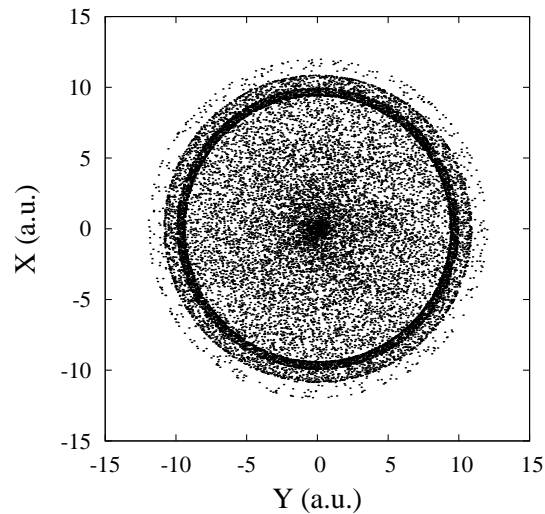
**Figure 5.** The distribution along the  $\Theta_y$  axis of protons channeled in the (11, 9) SWCNT with the image force taken into account – the solid curve – and without it – the dashed curve – when the proton incident angle  $\varphi = 10$  mrad. The proton velocity is  $v = 3$  a.u., the nanotube radius  $a = 0.689$  nm, and the nanotube length  $L = 0.2$   $\mu\text{m}$ . The former curve corresponds to the angular distribution shown in Fig. 4.

Fig. 2 gives the angular distribution of channeled protons for  $\varphi = 6$  mrad with the image force included. One can notice easily about a half of a ring-like structure, with an exceptionally high yield of channeled protons. This is the precursor of the effect known as the donut effect, which is connected to the misalignment of the proton beam and nanotube axis. In addition, the angular distribution contains several intricately shaped regions with lower yields of channeled protons. We show in Fig. 3 the corresponding distribution of channeled protons along the  $\Theta_y$  axis with and without the image force included. The sharp maximum of this distribution, appearing at  $-6.0$  mrad, is due to





**Figure 6.** The rainbow lines in the scattering angle plane for the protons channeled in the (11, 9) SWCNT with the inclusion of the image force when the proton incident angle  $\varphi = 10$  mrad. The proton velocity is  $v = 3$  a.u., the nanotube radius  $a = 0.689$  nm, and the nanotube length  $L = 0.2 \mu\text{m}$ .



**Figure 7.** The spatial distribution of protons channeled in the (11, 9) SWCNT with the image force included when the proton incident angle  $\varphi = 0$ . The proton velocity is  $v = 3$  a.u., the nanotube radius  $a = 0.689$  nm, and the nanotube length  $L = 0.2 \mu\text{m}$ .

the donut effect. It is evident that the image force makes this maximum weaker. On the other hand, the origin of the broad maximum of the distribution, located at  $-5.1$  mrad, is solely the image force. Thus, we can conclude that for the median values of  $\varphi$ , between 0 and about  $\psi_c/2$ , the image force still plays a significant role in generating the angular distribution.

We show in Fig. 4 the angular distribution of channeled protons for  $\varphi = 10$  mrad with the image force included. One can see clearly the whole ring-like structure, with

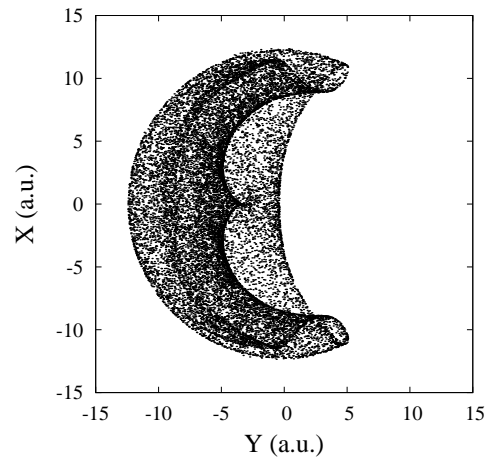


**Figure 8.** The spatial distribution of protons channeled in the (11, 9) SWCNT with the inclusion of the image force when the proton incident angle  $\varphi = 10$  mrad. The proton velocity is  $v = 3$  a.u., the nanotube radius  $a = 0.689$  nm, and the nanotube length  $L = 0.2$   $\mu\text{m}$ .

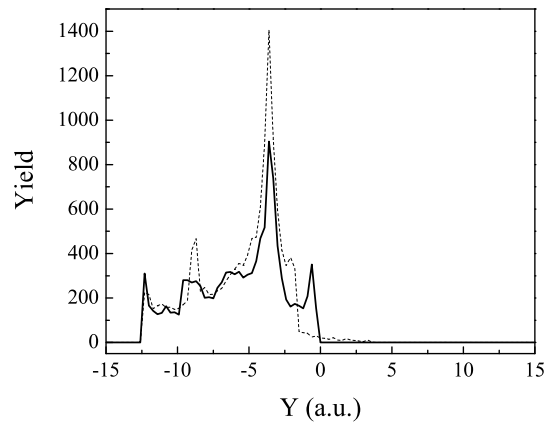


**Figure 9.** The distribution along the  $Y$  axis of protons channeled in the (11, 9) SWCNT with the image force taken into account – the solid curve – and without it – the dashed curve – when the proton incident angle  $\varphi = 10$  mrad. The proton velocity is  $v = 3$  a.u., the nanotube radius  $a = 0.689$  nm, and the nanotube length  $L = 0.2$   $\mu\text{m}$ . The former curve corresponds to the spatial distribution given in Fig. 8.

an exceptionally high yield of channeled protons. This is the fully developed donut effect. As it has been already said, the corresponding value of  $\varphi$  is close to the value of  $\psi_c$ . In addition, as in Fig. 2, the angular distribution contains several intricately shaped regions with lower but distinctly graded yields of channeled protons, with the very clear boundaries between them. Fig. 5 gives the corresponding distribution of channeled protons along the  $\Theta_y$  axis with and without the image force included. It is evident that, when  $\varphi$  is close to  $\psi_c$ , the role of the effect of dynamic polarization in generating the angular distribution is almost negligible. Fig. 6 shows the corresponding rainbow lines in the scattering angle plane with the dynamic polarization effect taken into account. These lines clearly demonstrate that the non-uniformity of the angular

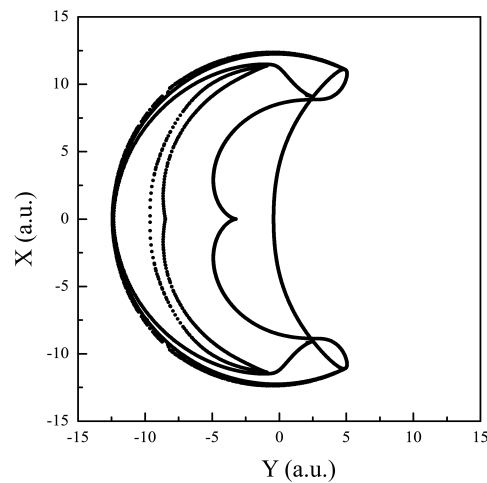


**Figure 10.** The rainbow lines in the final transverse position plane for the protons channeled in the (11, 9) SWCNT with the image force included when the proton incident angle  $\varphi = 10$  mrad. The proton velocity is  $v = 3$  a.u., the nanotube radius  $a = 0.689$  nm, and the nanotube length  $L = 0.2$   $\mu\text{m}$ .

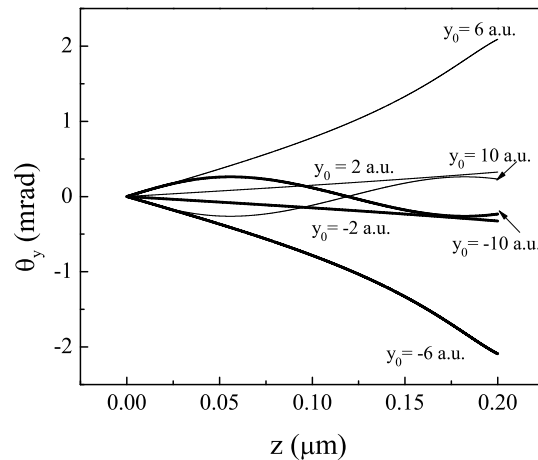


**Figure 11.** The dependence of the  $y$  component of the proton scattering angle on the  $z$  component of its position in the channeling through the (11, 9) SWCNT with the inclusion of the image force when the proton incident angle  $\varphi = 0$  for the  $x$  component of the proton impact parameter  $x_0 = 0$  and the  $y$  component of its impact parameter  $y_0 = \pm 2, \pm 6$  and  $\pm 10$  a.u. The proton velocity is  $v = 3$  a.u., the nanotube radius  $a = 0.689$  nm, and the nanotube length  $L = 0.2$   $\mu\text{m}$ .

distribution, including the donut effect, is due to the rainbow effect.

In Figs. 7-10 we shall display the evolution of the spatial distribution of channeled protons with the increase of  $\varphi$ , which is going on in parallel with the evolution of the angular distribution displayed in Figs. 1-6.

The scatter plot given in Fig. 7 represents the spatial distribution of channeled protons for  $\varphi = 0$  with the image force included. This spatial distribution and the corresponding spatial distribution without the image force included were analyzed in one of our previous papers [31]. We presented in it the distributions of channeled

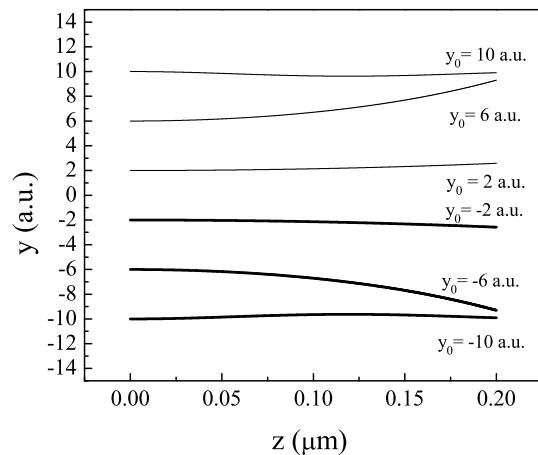


**Figure 12.** The dependence of the  $y$  component of the proton position on the  $z$  component of its position in the channeling through the (11, 9) SWCNT with the inclusion of the image force when the proton incident angle  $\varphi = 0$  for the  $x$  component of the proton impact parameter  $x_0 = 0$  and the  $y$  component of its impact parameter  $y_0 = \pm 2, \pm 6$  and  $\pm 10$  a.u. The proton velocity is  $v = 3$  a.u., the nanotube radius = 0.689 nm, and the nanotube length  $L = 0.2 \mu\text{m}$ .

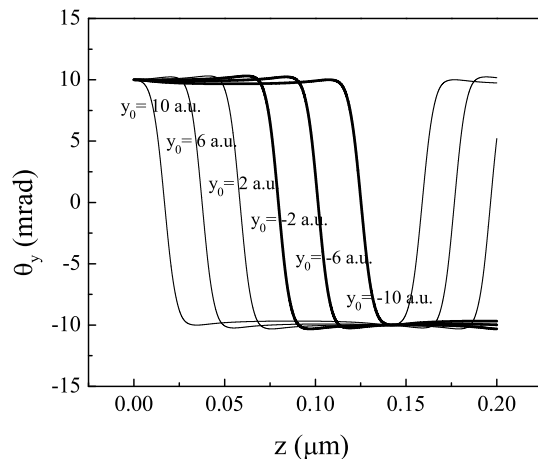


**Figure 13.** The dependence of the  $y$  component of the proton scattering angle on the  $z$  component of its position in the channeling through the (11, 9) SWCNT with the inclusion of the image force when the proton incident angle  $\varphi = 10$  mrad for the  $x$  component of the proton impact parameter  $x_0 = 0$  and the  $y$  component of its impact parameter  $y_0 = \pm 2, \pm 6$  and  $\pm 10$  a.u. The proton velocity is  $v = 3$  a.u., the nanotube radius  $a = 0.689$  nm, and the nanotube length  $L = 0.2 \mu\text{m}$ .

protons along the  $y$  axis with and without the image force included, which were in fact (for  $\varphi = 0$ ) the radial yields of channeled protons. It was demonstrated that the maxima of the radial yields, present in both spatial distributions, were the rainbow maxima. We also concluded that the dynamic polarization effect caused the shifts of the maxima of the spatial distribution generated with the effect not taken into account as well as the appearance of the additional maxima.

The spatial distribution of channeled protons for  $\varphi = 10$  mrad with the effect of

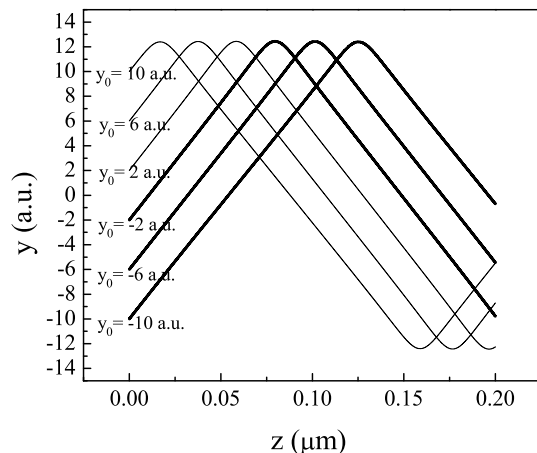


**Figure 14.** The dependence of the  $y$  component of the proton position on the  $z$  component of its position in the channeling through the (11, 9) SWCNT with the image force taken into account when the proton incident angle  $\varphi = 10$  mrad for the  $x$  component of the proton impact parameter  $x_0 = 0$  and the  $y$  component of its impact parameter  $y_0 = \pm 2, \pm 6$  and  $\pm 10$  a.u. The proton velocity is  $v = 3$  a.u., the nanotube radius  $a = 0.689$  nm, and the nanotube length  $L = 0.2$   $\mu\text{m}$ .

dynamic polarization taken into account is presented in Fig. 8. When this spatial distribution is compared to the spatial distribution for  $\varphi = 0$ , it is evident that the maximal change of  $\varphi$  induces a significant rearrangement of the protons in the final transverse position plane. Almost all the protons are displaced to the left half of the nanotube. However, as in the cases of angular distributions for  $\varphi = 6$  and  $10$  mrad, the spatial distribution also contains several intricately shaped regions with lower but distinctly graded yields of channeled protons, with the very clear boundaries between them. Fig. 9 gives the corresponding distribution of channeled protons along the  $Y$  axis, in the final transverse position plane, with and without the image force included. For this value of  $\varphi$ , the strongest maximum of the spatial distribution lies at  $-3.6$  a.u. instead at the origin for  $\varphi = 0$ . One can also conclude that, when  $\varphi$  is close to  $\psi_c$ , the role of the effect of dynamic polarization in generating the spatial distribution is small but noticeable. The effect makes the strongest maximum of the spatial distribution weaker and induces a rightward shift of the second strongest maximum. Fig. 10 shows the corresponding rainbow lines in the final transverse position plane with the image force taken into account. As in the case of angular distribution for this value of  $\varphi$ , these lines clearly demonstrate that the non-uniformity of the spatial distribution is to be attributed to the rainbow effect.

In Figs. 11-14 we shall display the typical proton trajectories through the nanotube in the proton phase space, complementing the result displayed in Figs. 1-10.

We show in Fig. 11 the  $y$  component of the proton scattering angle ( $\Theta_y$ ) as a function of the  $z$  component of its position within the nanotube with the effect of dynamic polarization included when  $\varphi = 0$  for  $x_0 = 0$  and  $y_0 = \pm 2, \pm 6$  and  $\pm 10$  a.u. Looking at the angular distribution shown in Fig. 1, we see that the channeled protons

with the impact parameters close to the nanotube axis, i.e., for  $y_0 = \pm 2$  a.u., and to the nanotube wall, i.e., for  $y_0 = \pm 10$  a.u., contribute to the part of the angular distribution close to the origin. The channeled protons with the impact parameters comparable to  $a/2$ , i.e., for  $y_0 = \pm 6$  a.u., give rise to the rainbow maxima lying at about 2 mrad.

Fig. 12 gives the dependence of the  $y$  component of the proton position on the  $z$  component of its position within the nanotube with the image force included when  $\varphi = 0$  for the same values of the components of the proton impact parameter as in Fig. 11. One can see that the channeled protons with  $y_0 = \pm 2$  a.u. give rise to the part of the spatial distribution close to the origin. The channeled protons with  $y_0 = \pm 6$  and  $\pm 10$  a.u. contribute to the peripheral part of the spatial distribution.

We give in Fig. 13 the  $y$  component of the proton scattering angle ( $\Theta_y$ ) as a function of the  $z$  component of its position with the image force taken into account when  $\varphi = 10$  mrad for the same values of the components of the proton impact parameter as in Fig. 11. It is easy to conclude that the channeled protons with  $y_0 = 2, 6$  and  $10$  a.u. contribute to the right part of the donut. The channeled protons with  $y_0 = -2, -6$  and  $-10$  a.u. give rise to the most intense part of the donut, being its farthest left part.

Fig. 14 shows the dependence of the  $y$  component of the proton position on the  $z$  component of its position with the image force included when  $\varphi = 10$  mrad for the same values of the components of the proton impact parameter as in Fig. 11. It is evident that all the propagating protons in question end up in the left half of the nanotube, after being reflected from the right part of the nanotube wall.

An additional result of our computer simulations is related to the influence of the image force on  $\psi_c$ . We followed the change of the total yield of channeled protons with the increase of  $\varphi$ , and found that with the image force taken into account  $\psi_c = 10.6$  mrad. When the image force is not taken into account  $\psi_c = 11.9$  mrad. This increase of  $\psi_c$  is attributed to the increase of the total interaction potential in question, given by Eq. (2), when its attractive component, originating in the interaction of the proton and its image, is not taken into account. This conclusion is justified via the relation between  $\psi_c$  and the total interaction potential at the distance from the nanotube wall equal to the screening radius,  $U_{SC}$ ,

$$\psi_c = \sqrt{\frac{U_{sc}}{E}}, \quad (10)$$

where  $E$  is the initial proton energy [49].

#### 4. Concluding remarks

We have presented the first theoretical investigation of the angular and spatial distributions of ions channeled through a nanotube for different proton incidence angles with the effect of dynamic polarization of the nanotube included. The ions are protons of the velocity of  $v = 3$  a.u. and the nanotube is an (11, 9) SWCNT of the length of  $L = 0.2 \mu\text{m}$ . The proton incident angle,  $\varphi$ , is varied between 0 and 10 mrad, being close

to the critical angle for channeling,  $\psi_c$ . We have noticed a slight increase of  $\psi_c$  when the image force is not taken into account.

We have observed a ring-like structure developing in the angular distribution of channeled protons with  $\varphi$  increasing and approaching  $\psi_c$ . The effect has been recognized as the donut effect, being in fact the rainbow effect. If  $\varphi$  is between 0 and about  $\psi_c/2$ , the image force plays a significant role in generating the angular and spatial distributions, including the rainbow maxima. However, if  $\varphi$  is close to  $\psi_c$ , the contribution of the image force to the angular and spatial distributions, including the donut effect, is minor.

The analysis of the generated spatial distributions of channeled protons has shown that the increase of  $\varphi$  can give rise to a significant rearrangement of the propagating protons within the nanotube. For example, for  $\varphi = 10$  mrad, the proton beam is displaced from the nanotube axis toward the nanotube wall leaving the region around the axis practically empty. It is clear that such a rearrangement of the propagating protons may be used to locate various atomic impurities in the nanotube, using the secondary processes like backward Coulomb scattering and nuclear reactions. In addition, the presence of the rainbow maxima in the spatial distributions can be used to determine the positions of the impurities very precisely. One can also think about directing such a nonosized proton beam to a material to be modified with it, or to a biological or medical sample.

## Acknowledgments

D. B., S. P., and N. N. acknowledge the support of the Ministry of Science and Technological Development of Serbia to the project *Physics and Chemistry with Ion Beams* (No. 451-01-00049), D. J. M. acknowledges the support of NABIIT and Danish Center for Scientific Computing (No. HDW-1103-06), while Z. L. M. acknowledges the support of NSERC.

## References

- [1] Artru X, Fomin S P, Shulga N F, Ispirian K A and Zhevago N K 2005 Carbon nanotubes and fullerites in high-energy and X-ray physics *Phys. Rep.* **412** 89
- [2] Mišković Z L 2007 Ion Channeling through Carbon Nanotubes *Radiat. Eff. Def. Solids* **162** 185
- [3] Moura C S and Amaral L 2007 Carbon nanotube ropes proposed as particle pipes *Carbon* **45** 1802
- [4] Moura C S and Amaral L 2005 Channeling on Carbon Nanotubes: A Molecular Dynamics Approach *J. Phys. Chem. B* **109** 13515
- [5] Zheng L-P, Zhu Z-Y, Li Y, Zhu D-Z and Xia H-H 2008 Ion mass dependence for low energy channeling in single-wall nanotubes *Nucl. Instrum. Methods Phys. Res. B* **266** 849
- [6] Zheng L-P, Zhu Z-Y, Li Y, Zhu D-Z and Xia H-H 2008 Isotopic Mass Effects for Low-Energy Ion Channeling in Single-Wall Carbon Nanotubes *Journal of Physical Chemistry C* **112** 15204
- [7] Matyukhin S I and Frolenkov K Y 2007 Critical Parameters of Channeling in Nanotubes *Tech. Phys. Lett.* **33** (1) 58
- [8] Matyukhin S I 2009 Efficiency of Ion Deviation by Bent Carbon Nanotubes *Tech. Phys. Lett.* **35** 318

- [9] Biryukov V M and Bellucci S 2002 Nanotube diameter optimal for channeling of high-energy particle beam *Phys. Lett. B* **542** 111
- [10] Bellucci S, Biryukov V M and Cordelli A 2005 Channeling of high-energy particles in a multi-wall nanotube *Phys. Lett. B* **608** 53
- [11] Zhu Z, Zhu D, Lu R, Xu Z, Zhang W and Xia H 2005 The experimental progress in studying of channeling of charged particles along nanostructure *Proc. of the Int. Conf. on Charged and Neutral Particles Channeling Phenomena (Frascati, Italy)* vol 5974 (Bellingham, Washington: SPIE) p 13
- [12] Chai G, Heinrich H, Chow L and Schenkel T 2007 Electron transport through single carbon nanotubes *Appl. Phys. Lett.* **91** 103101
- [13] Berdinsky A S, Alegaonkar P S, Yoo J B, Lee H C, Jung J S, Han J H, Fink D and Chadderton L T 2008 Growth of carbon nanotubes in etched ion tracks in silicon oxide on silicon *Nano* **2** 59
- [14] Krasheninnikov A V and Nordlund K 2005 Multiwalled carbon nanotubes as apertures and conduits for energetic ions. *Phys. Rev. B* **71** 245408
- [15] Mowbray D J, Mišković Z L, Goodman F O and Wang Y-N 2004 Interactions of Fast Ions with Carbon Nanotubes: Two-Fluid Model. *Phys. Rev. B* **70** 195418
- [16] Mowbray D J, Mišković Z L, Goodman F O and Wang Y-N 2004 Wake effect in interactions of fast ions with carbon nanotubes. *Phys. Lett. A* **329** 94
- [17] Zhou D-P, Wang Y-N, Wei L and Mišković Z L 2005 Dynamic Polarization Effects in Ion Channeling through Single-Wall Carbon Nanotubes *Phys. Rev. A* **72** 023202
- [18] Arista N R 2001 Interaction of ions and molecules with surface modes in cylindrical channels in solids *Phys. Rev. A* **64** 032901
- [19] Arista N R and Fuentes M A 2001 Interaction of charged particles with surface plasmons in cylindrical channels in solids *Phys. Rev. B* **63** 165401
- [20] Tökési K, Wirtz L, Lemell C and Burgdörfer J 2000 Charge-state evolution of highly charged ions transmitted through microcapillaries *Phys. Rev. A* **61** 020901(R)
- [21] Tökési K, Wirtz L, Lemell C and Burgdörfer J 2001 Hollow-ion formation in microcapillaries *Phys. Rev. A* **64** 042902
- [22] Tökési K, Tong X M, Lemell C and Burgdörfer J 2005 Energy loss of charged particles at large distances from metal surfaces *Phys. Rev. A* **72** 022901
- [23] Yamazaki Y 2007 Interaction of slow highly-charged ions with metals and insulators *Nucl. Instrum. Methods Phys. Res. B* **258** 139
- [24] Radović I, Hadžievski Lj, Bibić N and Mišković Z L 2007 Dynamic-polarization forces on fast ions and molecules moving over supported graphene *Phys. Rev. A* **76** 042901
- [25] Radović I, Hadžievski Lj and Mišković Z L 2008 Polarization of supported graphene by slowly moving charges *Phys. Rev. B* **77** 075428
- [26] Mowbray D J, Mišković Z L and Goodman F O 2006 Ion Interactions with Carbon Nanotubes in Dielectric Media *Phys. Rev. B* **74** 195435
- [27] Mowbray D J, Mišković Z L and Goodman F O 2007 Dynamic Interactions of Fast Ions with Carbon Nanotubes in Water *Nucl. Instrum. Meth. Phys. Res. B* **256** 167
- [28] Borka D, Petrović S, Nešković N, Mowbray D J and Mišković Z L 2006 Influence of the dynamical image potential on the rainbows in ion channeling through short carbon nanotubes *Phys. Rev. A* **73** 062902
- [29] Borka D, Petrović S, Nešković N, Mowbray D J and Mišković Z L 2007 Influence of the dynamical polarization effect on the angular distributions of protons channeled in double-wall carbon nanotubes *Nucl. Instrum. Methods Phys. Res. B* **256** 131
- [30] Borka D, Mowbray D J, Mišković Z L, Petrović S and Nešković N 2008 Dynamic polarization effects on the angular distributions of protons channeled through carbon nanotubes in dielectric media *Phys. Rev. A* **77** 032903
- [31] Borka D, Mowbray D J, Mišković Z L, Petrović S and Nešković N 2008 Channeling of protons through carbon nanotubes embedded in dielectric media *J. Phys.: Condens. Matter* **20** 474212



- [32] Schüller A, Adamov G, Wethekam S, Maass K, Mertens A and Winter H 2004 Dynamic dependence of interaction potentials for keV atoms at metal surfaces *Phys. Rev. A* **69** 050901(R)
- [33] Schüller A, Wethekam S, Mertens A, Maass K, Winter H and Gärtner K 2005 Interatomic potentials from rainbow scattering of keV noble gas atoms under axial surface channeling *Nucl. Instrum. Meth. Phys. Res. B* **230** 172
- [34] Winter H and Schüller A 2005 Rainbow scattering under axial surface channeling *Nucl. Instrum. Methods Phys. Res. B* **232** 165
- [35] Chadderton L T 1970 Diffraction and channeling *J. Appl. Crystallogr.* **3** 429
- [36] Rosner J S, Gibson W M, Golovchenko J A, Goland A N and Wegner H E 1978 Quantitative study of the transmission of axially channeled protons in thin silicon crystals *Phys. Rev. B* **18** 1066
- [37] Andersen S K, Fich O, Nielsen H, Schitt H E, Uggerhøj E, Vraast Thomsen C, Charpak G, Petersen G, Sauli F, Ponpon J P and Siffert P 1980 Influence of channeling on scattering of 2-15 GeV/c protons,  $\pi^+$ , and  $\pi^-$  incident on Si and Ge crystals *Nucl. Phys. B* **167** 1
- [38] Nešković N, Petrović S, Borka D and Kossionides S 2002 Rainbows with a tilted  $\langle 111 \rangle$  Si very thin crystal *Phys. Lett. A* **304/3-4** 114
- [39] Borka D, Petrović S and Nešković N 2003 Doughnuts with a  $\langle 110 \rangle$  very thin Si crystal, *Journal of Electron Spectroscopy and Related Phenomena* *Journal of Electron Spectroscopy and Related Phenomena* **129** 183
- [40] Petrović S, Miletić L and Nešković N 2000 Theory of rainbows in thin crystals: the explanation of ion channeling applied to  $\text{Ne}^{10+}$  ions transmitted through a  $\langle 100 \rangle$  Si thin crystal *Phys. Rev. B* **61** 184
- [41] Petrović S, Borka D and Nešković N 2005 Rainbows in transmission of high energy protons through carbon nanotubes. *Eur. Phys. J. B* **44** 41
- [42] Petrović S, Borka D and Nešković N 2005 Rainbow effect in channeling of high energy protons through single-wall carbon nanotubes *Nucl. Instrum. Methods Phys. Res. B* **234** 78
- [43] Borka D, Petrović S and Nešković N 2005 Rainbow effect in channeling of high energy protons in (10, 0) single-wall carbon nanotubes *Mat. Sci. For.* **494** 89
- [44] Nešković N, Petrović S and Borka D 2005 Angular distributions of 1 GeV protons channeled in bent short single-wall carbon nanotubes *Nucl. Instrum. Methods Phys. Res. B* **230** 106
- [45] Zhevago N K and Glebov V I 1998 Channeling of fast charged and neutral particles in nanotubes *Phys. Lett. A* **250** 360
- [46] Doyle P A and Turner P S 1968 Relativistic Hartree-Fock X-ray and electron scattering factors *Acta Crystallogr. A* **24** 390
- [47] Lindhard J. K 1965 Influence of crystal lattice on motion of energetic charged particles *Dan. Vidensk. Selsk., Mat.-Fys. Medd.* **34**, No. 14, 1
- [48] Saito R, Dresselhaus G and Dresselhaus M S 2001 *Physical Properties of Carbon Nanotubes* (London: Imperial College Press)
- [49] Zhevago N K and Glebov V I 2003 Computer simulations of fast particle propagation through straight and bent nanotubes *Phys. Lett. A* **310** 301